Journal of Power Sources 195 (2010) 3569–3578

Contents lists available at ScienceDirect

Journal of Power Sources

journal homepage: www.elsevier.com/locate/jpowsour

On the performance of membraneless laminar flow-based fuel cells

Ranga S. Jayashree[a,1,2], Seong Kee Yoon[b,1], Fikile R. Brushett[a], Pedro O. Lopez-Montesinos[a], Dilip Natarajan[c], Larry J. Markoski[c], Paul J.A. Kenis[a,b,*]

[a] Department of Chemical & Biomolecular Engineering, University of Illinois at Urbana-Champaign, 600 S. Mathews Ave., Urbana, IL 61801, United States
[b] Department of Mechanical Science & Engineering, University of Illinois at Urbana-Champaign, 1206 W. Green St., Urbana, IL 61801, United States
[c] INI Power Systems, 175 Southport Drive - Suite 100, Morrisville, NC 27560, United States

ARTICLE INFO

Article history:
Received 20 September 2009
Received in revised form 8 December 2009
Accepted 8 December 2009
Available online 16 December 2009

Keywords:
Laminar flow
Membraneless
Fuel cell
Fuel utilization
Hydrodynamic focusing
Fuel crossover

ABSTRACT

This paper reports on the characterization and optimization of laminar flow-based fuel cells (LFFCs) for both performance and fuel utilization. The impact of different operating conditions (volumetric flow rate, fuel-to-electrolyte flow rate ratio, and oxygen concentration) and of different cell dimensions (electrode-to-electrode distances, and channel length) on the performance (both power density and fuel utilization) of individual LFFCs is investigated. A finite-element-method simulation, which accounts for all relevant transport processes and electrode reactions, was developed to explain the experimental results here. This model can be used to guide further LFFC optimizations with respect to cell design and operation conditions. Using formic acid as the fuel, we measured a peak power density of 55 mW cm^{-2}. By hydrodynamically focusing the fuel to a thin stream on the anode we were able to reduce the fraction of fuel that passes through the channel without reacting, thereby increasing the fuel utilization per pass to a maximum of 38%. This paper concludes with a discussion on the various trade-offs between maximizing power density and optimizing fuel utilization per pass for individual LFFCs, in light of scaling out to a multichannel LFFC-based power source system.

1. Introduction

The desire for ever-increasing capabilities and longer off-the-grid run times for portable electronics (*i.e.*, laptops, cell phones, and PDAs) has spurred research and development of fuel cell-based power sources, which have the potential of achieving significantly higher energy densities than rechargeable batteries [1]. Over the past decade, several existing membrane-based fuel cell technologies, using hydrogen or small organics (*i.e.*, methanol, formic acid) as the fuel, have been miniaturized [2–4]. In addition, novel concepts and designs have been developed, including solid acid fuel cells [5], biofuel cells [6,7], microfabricated fuel cells [8–10], and membraneless fuel cells [11]. Hydrogen fueled polymer electrolyte membrane-based fuel cells (PEMFCs) are developed most extensively and have been implemented successfully in stationary and extraterrestrial applications [12,13]. These hydrogen PEMFCs are not considered viable for portable applications, however, due to safety concerns and practical challenges associated with high energy density storage of hydrogen fuel. On-board reforming of high energy density liquids to hydrogen is a possible alternative. However the required ancillary systems increase device complexity, hinder scalability, and reduce system energy density. A second alternative is the use of direct liquid fuel cells which benefit from the high energy density and easy storage of organic fuels [14].

Over the past decade or so, promising microscale direct formic acid fuel cells (DFAFCs) [3,8] and direct methanol fuel cells (DMFCs) [15] have been explored, yet their development is still hampered by technical challenges such as fuel crossover, anode dry-out, and cathode flooding [12]. To reduce fuel crossover, conventional DMFCs are operated at relatively low methanol concentrations (0.5–2 M), necessitating an ancillary system for diluting the highly concentrated or neat methanol stored in a fuel reservoir. Anode dry-out occurs while operating at high current densities due to the osmotic drag of water molecules along with protons transported across the membrane, from the anode to the cathode. Osmotic drag in combination with water formation causes flooding of the cathode, which hampers oxygen transport to electrocatalytic sites. One passive approach to overcome anode dry-out and cathode flooding is the application of a more hydrophobic polytetrafluoroethylene (PTFE) coating to the cathode and application of a more hydrophilic Nafion-based coating to the anode, both resulting in water being driven back to the anode side [16]. Compared to DMFCs, DFAFCs

* Corresponding author at: Department of Chemical & Biomolecular Engineering, University of Illinois at Urbana-Champaign, 600 S. Mathews Ave., Urbana, IL 61801, United States. Tel.: +1 217 265 0523.
E-mail address: kenis@illinois.edu (P.J.A. Kenis).
[1] Contributed equally to this work.
[2] Present address: P.O. Box 4098, Chemistry Department, Georgia State University, Atlanta GA 30302, United States.

0378-7753/$ – see front matter © 2010 Elsevier B.V. All rights reserved.
doi:10.1016/j.jpowsour.2009.12.029

Nomenclature

μ	dynamic viscosity
u	velocity vector
ρ	density
p	pressure
Δp_{cell}	pressure drop through the cell
D	diffusion coefficient
C	concentration
C_0	inlet concentration
i_0	exchange current density
n_{tot}	number of total electrons exchanged
n_l	number of electrons exchanged at the rate-limiting step
α_a	anode transfer coefficient
α_c	cathode transfer coefficient
η_a	anode overpotential
η_c	cathode overpotential
F	Faraday constant
R	Universal gas constant
T	temperature
k	rate constant
J_c	Bulter–Volmer flux at the cathode
R_{rxn}	formic acid oxidation reaction rate
n	normal vector
N	normal diffusion-convection vector
Q	total volumetric flow rate
u_0	linear velocity
y	channel length
H	channel height
δ	boundary layer thickness
Sc	Schmidt number
Re	Reynold's number

exhibit excellent electro-oxidation kinetics on Pd nanoparticle catalysts at room temperature [17] and are less prone to fuel crossover thus enabling the use of higher fuel concentrations [18]. The latter greatly simplifies the design of DFAFCs based power sources (*e.g.* passive fuel delivery) and overcomes the disadvantage of the lower energy density of formic acid vs. methanol (285.5 kJ mol^{-1} vs. 702.5 kJ mol^{-1}, respectively). Both DMFCs and DFAFCs still suffer from water management, and other membrane-related issues such as cost and durability, which has hampered commercialization efforts.

Due to the lack of turbulent mixing at the microscale, the laminar flow regime allows for multiple streams to be compartmentalized in a single microchannel with only diffusive mixing occurring at the liquid–liquid interface between the different streams [19]. We [20–27] and others [11,28–32] have exploited this phenomenon to create membraneless fuel cells. The laminar nature of flow eliminates the need for physical barrier such as a membrane, while still allowing for ionic transport between the anode and the cathode [11,20–23,27]. This membraneless architecture overcomes some of the aforementioned membrane-related issues: (i) fuel crossover can be minimized by adjusting cell dimensions and stream flow rates (*i.e.*, by operation at a high Péclet number, $Pe > 3000$) [21,27,33]; (ii) water management issues such as anode dry-out and cathode flooding are absent in this all-aqueous system; (iii) the composition of the fuel, electrolyte and oxidant streams can be specified independently, enabling LFFC operation with different fuels and different media (*i.e.*, acidic or alkaline), which enables optimization of reaction kinetics at the individual electrodes [22–24,26]; and (iv) by-products of fuel oxidation reactions (*i.e.*, carbonates formed under alkaline conditions) can be removed by the convecting streams.

Here, we present a detailed characterization and optimization of LFFC for both performance and fuel utilization. The effects of design and operation parameters (electrode-to-electrode distance, total flow rate, fuel-to-electrolyte flow rate ratio, oxygen concentration) on the power density of an individual direct formic acid LFFC are investigated. Hydrodynamic focusing, a well-known microfluidic approach used for a variety of purposes [34,35], is introduced as a strategy of increasing the fuel utilization per pass. To explain the experimental results, a finite-element-method simulation is developed, which accounts for all relevant transport and electrode processes. This model can aid further LFFC optimizations with respect to cell design and operation conditions. We conclude with a discussion on the various trade-offs between maximizing power density and optimizing fuel utilization per pass, especially in light of scaling out a single-channel LFFC into a multichannel power source.

2. Experimental

2.1. Electrode preparation and fuel cell assembly

In these studies, two LFFC configurations were used. In the first design, referred to a first generation LFFC or G1 LFFC, the aqueous fuel and oxidant streams flow in parallel in a single microchannel with the anode and cathode on opposing side walls (Fig. 1a). In the G1 LFFCs, graphite plates served as current collectors and catalyst support structures. The different anode and cathode catalysts were hand-painted onto the graphite plates. For the anode, catalyst composition of 10 mg cm^{-2} Pd black nanoparticles (Alfa Aesar, MA) and 1.5 mg cm^{-2} Nafion (used as a binder in all inks, 5 wt% solution, Dupont) and 10 mg cm^{-2} of Pt-Ru black nanoparticles (Alfa Aesar, MA) and 1.5 mg cm^{-2} Nafion were used for the formic acid and methanol LFFCs, respectively. For the cathode, a catalyst composition of 2 mg cm^{-2} Pt black (Alfa Aesar, MA) and 0.1 mg cm^{-2} Nafion was used. The two graphite plates were aligned to form a channel with 0.1-cm electrode-to-electrode distance (width), a 3-cm length, and a 0.1-cm height. The anolyte (fuel and electrolyte) and catholyte (oxidant and electrolyte) streams flow in a laminar fashion over the anode and cathode, respectively. The electrode area along a microchannel wall between the inlets and the outlet (3-cm long and 0.1-cm wide) is used as the geometric surface area of the electrodes in this study (0.3 cm^2). The multilayer assembly was held together with binder clips (Highmark). The design is described in further detail elsewhere [21].

In the second design, referred to as a second generation LFFC or G2 LFFC, a gas diffusion electrode (GDE) exposed to ambient air is used as an air-breathing cathode (Fig. 1b). Consequently, the two laminar streams in the microchannel are now an anolyte (fuel in aqueous electrolyte) and a catholyte (aqueous electrolyte only) flowing over the anode and cathode, respectively. In the G2 LFFC, a graphite plate with two inlets and one outlet served as the anode catalyst support and the current collector. Polyethylene tubes (Cole-Parmer, IL) were secured in the inlet and outlet holes with 5-min epoxy glue (Devcon, MA). For the anode, catalyst compositions of 10 mg cm^{-2} Pd black nanoparticles and 1.5 mg cm^{-2} Nafion and 10 mg cm^{-2} Pt–Ru alloy nanoparticles (Alfa Aesar, MA) and 1.5 mg cm^{-2} Nafion were used for the formic acid and methanol LFFCs, respectively. For the air-breathing cathode, catalyst ink consisting of 2 mg cm^{-2} Pt black nanoparticles and 0.1 mg cm^{-2} Nafion was hand-painted onto a EFCG "S" Type Electrode on Toray carbon paper with no catalyst (E-TEK, Somerset, NJ) to create a gas diffusion electrode (GDE). A 3-cm long and 0.3-cm wide window was precision-machined into a 0.2-cm thick polymethylmethacrylate (PMMA) sheet to serve as a spacer layer between the anode (graphite plate) and the cathode (GDE). The window forms the flu-

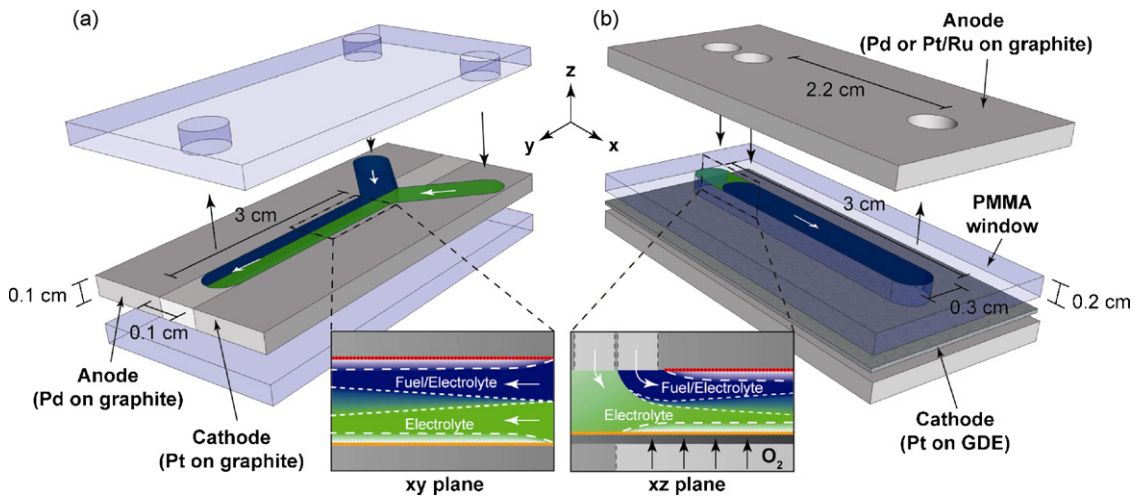

Fig. 1. Schematic designs of: (a) first generation LFFC (G1), operated by flowing a fuel stream (blue) and an oxygen-saturated electrolyte stream (green) in parallel; (b) second generation LFFC (G2) operated by flowing a fuel stream (blue) and an electrolyte stream (green) in parallel with the oxygen entering through a porous gas diffusion electrode (GDE) which serves as the cathode. The insets schematically show reaction depletion and diffusional mixing zones at the electrodes and at the liquid–liquid interface, respectively. (For interpretation of the references to color in this figure legend, the reader is referred to the web version of the article.)

idic channel between the anode and cathode through which the fuel and electrolyte streams flow in a laminar fashion. The electrode-to-electrode distance is set by the thickness of the PMMA window. The inlets and outlet of the graphite plate are exactly lined up with the ends of the microfluidic channel machined in the PMMA. The electrode area between the inlets and the outlet (2.2-cm long and 0.3-cm wide) is the geometric surface area of the electrodes used in this study (0.66 cm^2). A graphite window functioning as a current collector is placed over the GDE on the cathode side. Then, a second PMMA sheet with a window is positioned over this current collector. The windows machined in the current collector and PMMA sheet allow oxygen from air to reach the cathode. In the case of forced oxygen delivery, this second PMMA sheet is replaced with a polycarbonate chamber (5 (L) cm × 1 (W) cm × 0.5 (H) cm) so oxygen (laboratory grade, S. J. Smith) could be fed to the cathode at 50 sccm. The multilayered assembly is held together using binder clips (Highmark). Further details on the fabrication of this air-breathing LFFC can be found elsewhere [23].

2.2. Fuel cell testing

The assembled fuel cells were tested under acidic conditions. For both G1 and G2 LFFCs, the anode stream was 1 M formic acid (HCOOH) in 0.5 M sulfuric acid (H_2SO_4). For the G1 LFFC, the cathode stream was oxygen-saturated 0.5 M H_2SO_4. High purity oxygen (S.J. Smith, Laboratory grade) was bubbled, for 15 min, through a 0.5 M H_2SO_4 solution in a glass tube capped with a glass frit to aid with the solution saturation. For the G2 LFFCs, the cathodic GDE was either exposed to quiescent air or a forced oxygen stream (50 $cm^3\ s^{-1}$). For the latter experiments, a gas flow chamber (5 (L) cm × 1 (W) cm × 0.5 (H) cm) was precision-machined into a PMMA sheet which was then clamped over the cathode. Polarization curves were obtained by chronoamperometric measurements at different cell potentials using a potentiostat (Autolab PGSTAT-30, EcoChemie). Potentiostat leads were attached to the anodic and cathodic graphite current collectors via copper alligator clips. The working electrode lead was attached to the anode while the reference and counter electrode leads were combined and attached to the cathode. The potentiostat was used to generate an applied potential, and a multimeter (Fluke), with its leads attached to the anodic and cathodic graphite current collectors, was used to determine the actual cell potential. This measurement configuration eliminates any electrical contributions due to contact resistances between the alligator clips of the leads and the graphite current collector plates. The steady-state current measurements observed at each cell potential were recorded using General Purpose Electrochemical System (GPES) software (EcoChemie) provided with the potentiostat used. As previously mentioned, the exposed geometric surface area of the anode (0.3 and 0.66 cm^2 for the G1 and G2 LFFC, respectively) was used to calculate current and power densities. Fuel and electrolyte/oxidant stream flow rates were varied from 0.075 to 0.30 ml min^{-1} per stream (total stream flow rate of 0.15 to 0.6 ml min^{-1}) using a syringe pump (Harvard Apparatus). Upon exiting each fuel cell, the streams travel through polyethylene tubing (Cole Parmer) and collect in a beaker. By placing an external Ag/AgCl reference electrode (in 3 M NaCl, BAS, West-Lafayette, IN) individual electrode polarization curves could be independently monitored for each applied fuel cell potential [20]. Individual anode and cathode polarization was measured using two multimeters, functioning in voltmeter mode, attached to the reference electrode and each of the graphite plate current collectors. No potential drop occurred along the length of the tubing connecting the cell with the reference electrode. All experiments were performed at room temperature.

2.3. Fuel utilization studies

The polarization curves for formic acid G2 LFFCs with a 0.2-cm electrode-to-electrode distance were measured at total flow rates (cathode and anode streams) of 0.1 and 0.8 ml min^{-1}. For each of these total flow rates, the fuel-to-electrolyte flow-rate ratios were varied from 1:1 to 1:20. All experiments were performed at room temperature.

2.4. Modeling the physicochemical phenomena

To qualitatively assess the performance of both G1 and G2 LFFCs, we simulated a T-shaped LFFC geometry using three-dimensional finite-element-method software (FEMLAB 3.2 from Comsol) and varied fuel cell operating conditions. The simulations were carried out by coupling the following governing equations: the Navier Stokes equations (Eq. (1)), the continuity equation (Eq. (2)), and the species transport equation (Eq. (3)) while using the Butler–Volmer equation (Eq. (4)) to simulate the oxygen reduction reaction (ORR)

Table 1
Boundary conditions used to simulate dissolved oxygen concentration profiles within G1 LFFC.

Boundary conditions to solve Eqs. (1) and (2)
$\mathbf{u} = (u_0, 0, 0)$, where u_0 is the inlet velocity
$\mathbf{u} = (0, 0, 0)$ at the walls
$p = 0$ at the outlet (at inlet, $p = \Delta p_{cell}$)
Boundary conditions to solve Eq. (3)
$C = C_0$ at the cathode inlet
$C = 0$ at the anode inlet
$(-D\nabla C + C\mathbf{u})\cdot\mathbf{n} = 0$ at the walls
$(-D\nabla C + C\mathbf{u})\cdot\mathbf{n} = C\mathbf{u}\cdot\mathbf{n}$ at the outlet
$\mathbf{n}\cdot\mathbf{N} = J$ at cathode surface[a]

[a] $\mathbf{N} = -D\nabla C + C\mathbf{u}$ and J is an outward flux imposed at the reactive wall using Eq. (4).

Table 2
Boundary conditions used to simulate formic acid concentration profiles within a G2 LFFC.

Boundary conditions to solve Eqs. (1) and (2)
$\mathbf{u} = (u_0, 0, 0)$, where u_0 is the inlet velocity
$\mathbf{u} = (0, 0, 0)$ at the walls
$p = 0$ at the outlet (at inlet $p = \Delta p_{cell}$)
Boundary conditions to solve Eq. (3)
$C = C_0$ at the anode inlet
$C = 0$ at the cathode inlet
$(-D\nabla C + C\mathbf{u})\cdot\mathbf{n} = 0$ at the walls
$(-D\nabla C + C\mathbf{u})\cdot\mathbf{n} = C\mathbf{u}\cdot\mathbf{n}$ at the outlet
$\mathbf{n}\cdot\mathbf{N} = R_{rxn}$ at anode surface[a]

[a] $\mathbf{N} = -D\nabla C + C\mathbf{u}$ and R_{rxn} is an outward flux imposed at the reactive wall using Eq. (5).

at the cathode and the formic acid oxidation reaction on the anode was simulated using a rate law (Eq. (5)) [1].

$$-\nabla \cdot \mu(\nabla \mathbf{u} + (\nabla \mathbf{u})^T + \rho(\mathbf{u}\cdot\nabla)\mathbf{u} + \nabla p = 0 \quad (1)$$

$$\nabla \cdot \mathbf{u} = 0 \quad (2)$$

$$\nabla \cdot (-D\nabla C + C\mathbf{u}) = 0 \quad (3)$$

$$J_c = \left(\frac{i_0}{n_{tot}F}\right)\left(\frac{C}{C_0}\right)\left[\exp\left(\frac{\alpha_c n_1 F\eta_c}{RT}\right) - \exp\left(\frac{-\alpha_c n_1 F\eta_c}{RT}\right)\right] \quad (4)$$

$$R_{rxn} = (kC)\exp\left(\frac{\alpha_c n_1 F\eta_c}{RT}\right) \quad (5)$$

The boundary conditions used to solve for G1 and G2 LFFC (vide infra) are shown in Tables 1 and 2, respectively. To solve the strongly coupled multiphysics problem a set of assumptions were made: (i) fluids are Newtonian and of constant density and viscosity; (ii) fluids are dilute solutions thus density can be approximated as that of water and Fick's law applies; (iii) fluid flow is stead; (iv) because flow is in the laminar regime (*i.e.*, $Re < 10$ for LFFCs), viscous effects dominate and inertial effects have a minimal impact; and (v) body forces are negligible. The above equations were solved simultaneously in a single domain; a T-shaped channel geometry. For simplicity, we approximated the LFFC architecture as a T-junction governed by Eqs. (1)–(3) except for the walls covered with electrodes, where Eqs. (4) and (5) are imposed as electrode boundary conditions. Modeling was used to investigate the impact of different species on cell performance, namely dissolved oxygen in a G1 LFFC and formic acid in a G2 LFFC. Studies were performed at a cell potential of 0.3 V, where peak power density is observed. All critical input data, compiled from references [29,36,37], is shown in Table 3.

For the G1 LFFC studies (Section 3.1), concentration profiles of dissolved oxygen (in water) are generated along the channel length in the *x*–*y* plane, as well as across the channel at three cross-sections in the *x*–*z* plane. The boundary conditions used to solve the relevant

Table 3
Input values of the constants and variables for the simulations.

Parameter	Values used	Units
ρ	1×10^3 (water)	kg m^{-3}
μ	1×10^{-3} (water)	kg m^{-1} s^{-1}
u_0	±0.0008–0.0050	m s^{-1}
Q	0.075–0.300	ml min^{-1}
C_0	2.5×10^{-3} (oxygen)	M
	1 (formic acid)	
D	2×10^{-9} (oxygen)	m^2 s^{-1}
	5×10^{-10} (formic acid)	
T	298	K
n_l	1 (oxygen)	–
	1 (formic acid)	
K	1×10^{-2} (formic acid)	cm s^{-2}
i_0	5.7×10^{-3} (oxygen)	A cm^{-2}
η	0.6 (oxygen)	V
	0.6 (formic acid)	
R	8.31	J mol^{-1} K^{-1}
α	0.500 (oxygen)	–
	0.497 (formic acid)	
F	96485	C

equations are detailed in Table 1. For these studies, the channel length, width and height are 2.5, 0.1, and 0.1 cm, respectively. These dimensions are similar to those of the G1 LFFC shown in Fig. 1a. The inlet dissolved oxygen concentration is 2.5 mM and the total inlet flow rate is 0.1 ml min^{-1}. In addition, a current density profile of the oxygen reduction reaction at the cathode was also included (Fig. 2b).

For the G2 LFFC studies (Section 3.3), formic acid concentration profiles are generated along the channel length using different flow conditions. Specifically, the total flow rate and the volumetric fuel-to-electrolyte ratio were varied. The boundary conditions used to solve the relevant equations are detailed in Table 2. For these studies, the channel length, width and height are 2.5, 0.2, and 0.2 cm, respectively. These dimensions are similar to those of the actual G2 LFFC shown in Fig. 1b and used in the experimental studies. Fuel utilization fractions are calculated using these simulated concentration profiles by taking the difference of the mass flux of the inlet and outlet fuel streams and dividing by the total mass flux of fuel at the inlet. The calculated fuel utilization data is then qualita-

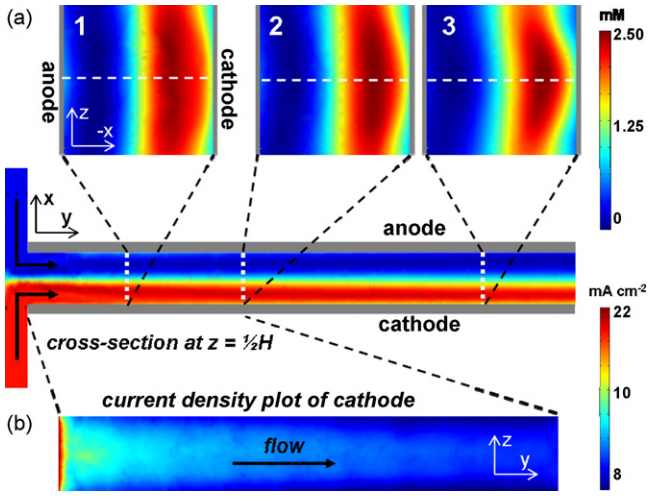

Fig. 2. (a) FEMLAB concentration profiles of oxygen-saturated solution, entering in the cathode stream at a concentration of 2.5 mM. The T-shaped cross-section (*x*–*y* plane) cuts through the channel at $Z = (1/2)H$, the center of the channel with height *H*. The cross-sections (*x*–*z* plane) 1, 2, 3 are taken at 0.5, 1 and 2 cm down the channel, respectively, perpendicular to the direction of flow. (b) Visualization of the simulated current density on the surface of the cathode. For these simulations, the channel length, width and height are 2.5, 0.1, and 0.1 cm, respectively.

tively compared to experimental data from a G2 LFFC (vide infra). The inlet formic acid concentration is 1 M HCOOH. The inlet flow rates were set to 0.05 ml min^{-1} for each inlet for the 1:1 fuel-to-electrolyte flow rate ratio, and to 0.0111 and 0.0889 ml min^{-1} for the 1:8 flow-rate ratio.

3. Results and discussion

3.1. G1 LFFC; dissolved oxidant

The performance of the G1 LFFCs using a fuel stream of 1 M HCOOH + 0.5 M H_2SO_4, and an oxidant stream of oxygen-saturated 0.5 M H_2SO_4 was investigated as previously reported [21]. Fig. 3 shows typical polarization and power density curves obtained with the G1 LFFC using formic acid as the fuel. In prior work, the sharp potential drop observed at current densities of ~13 mA cm^{-2} is due to mass transport limitations that originate at the cathode side [20,21,23]. Furthermore, the fuel utilization calculated for these G1 LFFCs at a cell potential of 0.3 V, where maximum power density is achieved, is only 0.04% per pass, clearly insufficient for any meaningful application. Use of a higher energy density oxidant such as potassium permanganate can overcome the mass transport limitation at the cathode [21], but the volume required to transport oxidant in addition to the fuel would reduce the overall system energy density of any fuel cell-based power source. An alternative approach to overcoming the mass transfer limitation could be using perfluorinated hydrocarbon emulsions as the electrolyte to increase oxygen solubility [38], but emulsion instability and catalyst fouling renders this approach less attractive.

To better understand the performance-limiting cathode characteristics of the G1 LFFC, specifically the diffusion and reaction of dissolved oxygen along the channel length, we employed a three-dimensional FEMLAB simulation. To solve this model all the relevant physical and chemical processes, described in Section 2.4, were taken into account. Prior work (also *vide supra*) indicates that G1 LFFCs are cathode limited [21], so the Butler–Volmer equation was used on the cathode for the rate-limiting, one electron step of the oxygen reduction reaction (ORR) [29]. To maintain overall electro-neutrality, the actual rate of fuel electro-oxidation at the anode equal to the rate-limiting ORR at the cathode by adjusting the rate constant k for the anode reaction.

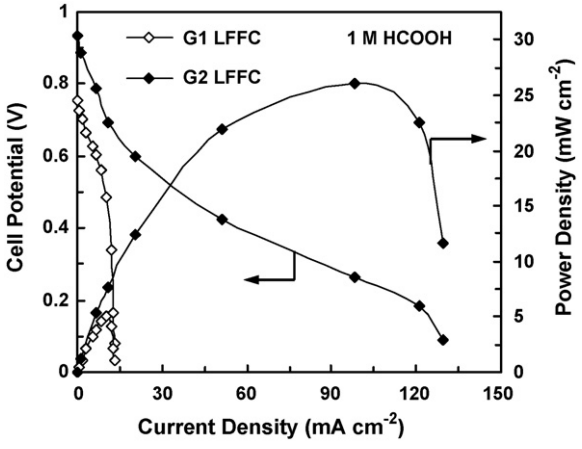

Fig. 3. (a) Polarization and power density curves obtained with formic acid G1 and G2 LFFCs. The anode stream was 1 M HCOOH + 0.5 M H_2SO_4 for both LFFCs. The cathode stream was 0.5 M H_2SO_4 saturated with dissolved oxygen for the G1 LFFC and 0.5 M H_2SO_4 with an air-breathing cathode for the G2 LFFC. In all studies, the anode and cathode stream flow rates were 0.3 ml min^{-1} each (0.6 ml min^{-1} total flow rate) and experiments were performed at room temperature.

Fig. 2a shows oxygen concentration profiles within the G1 LFFC: a cross-sectional view along the length of the channel as well as three cross-sectional views perpendicular to the direction of flow at different positions along the channel. The color gradients clearly visualize diffusional broadening at the liquid–liquid interface as well as growth of the depletion boundary layer from the leading edge of the cathode. The pressure driven, parabolic profile characteristic for laminar flow causes the depletion boundary layer thickness to be up to eight times greater in the corners than in the middle of the channel. The presence of the depletion boundary layer and the low oxygen solubility in aqueous media (typically >5 mM) limits the performance of G1 LFFCs to the levels observed experimentally (Fig. 3) unless a more soluble oxidant is used such as potassium permanganate [21]. In addition to oxygen concentration profiles the simulation also provides information on the current density along the cathode surface (Fig. 2b). As expected, most of the reaction occurs on the electrode surface closest to the leading edge at the inlet and at the middle of the channel since the depletion boundary layer is thinnest at these locations.

LFFC performance also depends on the extent of fuel (or oxidant) crossover due to diffusional broadening at the liquid–liquid interface in the channel center, as shown for oxygen in Fig. 2a. As previously reported, the shape and width of the diffusional mixing zone at a liquid–liquid interface depends on the operating conditions as defined by the Péclet number, the ratio of inertia and dispersion [33]. Later in this article, the extent of fuel crossover in LFFCs under different operation conditions will be investigated and strategies to minimize this phenomenon and maximize LFFC performance, in particular G2 LFFC performance, will be highlighted.

3.2. G2 LFFC; air-breathing cathode

To overcome the aforementioned cathode limitations in the G1 LFFCs, an air-breathing cathode GDE was introduced (Fig. 1b) [23]. As oxygen is now supplied to the cathode directly from ambient environment, the cathode stream is only a conductive electrolyte (here 0.5 M H_2SO_4) that serves as a barrier to fuel crossover. The air-breathing configuration benefits from a higher oxygen concentration in air compared to in a saturated aqueous solution (~10 mM vs. ~2 mM, respectively), and a significantly improved oxygen diffusion constant in air compared to in solution (2×10^{-1} cm^2 s^{-1} vs. 2×10^{-5} cm^2 s^{-1}, respectively). These improvements overcome the mass transport issues encountered in G1 LFFCs as evidenced by the enhanced performance at high current densities in G2 LFFCs (Fig. 3). A fivefold increase in peak power density, from 5 to 26 mW cm^{-2}, was observed when operating a G2 LFFC with 1 M HCOOH compared to a G1 LFFC operated under identical conditions. Note that in both LFFC architectures, the fuel electro-oxidation at the anode generated gaseous carbon dioxide but these bubbles were washed away by the flowing streams prior to growing large enough to disturb the laminar regime.

3.3. Fuel utilization

Fuel crossover is an issue in conventional DMFCs and, to a lesser extent, DFAFCs, causing a mixed potential at the cathode which reduces cell performance and fuel utilization. In LFFCs, fuel crossover is governed by diffusive mixing and can be controlled by altering stream flow rates and varying channel dimensions. However, adjusting these operational and structural parameters lead to trade-offs between maximizing power density and fuel utilization. For example, by increasing stream flow rates, the extent of fuel crossover can be minimized as the decreased residence time will decrease the extent of diffusional broadening. An increase in flow rate improves cell performance by minimizing both fuel crossover and boundary layer thickness, but it also reduces fuel utilization

as the shortened residence time gives the fuel less time to diffuse to and react at the anode. Vice versa, decreasing stream flow rates will increase fuel utilization, but reduce power density. A different solution is needed.

Previously, we have reported a method to increase the conversion yield of an electrochemical microreactor by hydrodynamically focusing the reactants into a thin stream on the electrode [35]. The same hydrodynamic focusing concept [34] can be applied to increase the fuel utilization in LFFCs. In Fig. 4, the optical micrographs highlight how the fuel–electrolyte interface can be shifted from the center of the channel towards either electrode by adjusting the flow rate ratio between the two streams. In LFFCs, focusing of the fuel stream close to the anode will aid in reducing fuel crossover (larger diffusion distance to the cathode) as well as in increasing fuel utilization. The impact of shifting these liquid–liquid interfaces on diffusive broadening, depletion layer formation and electrode utilization can be modeled using cross-channel formic acid (fuel) concentration profiles as a function of distances down the channel. In these simulations the LFFC is operated at peak power density, which is observed at 0.3 V. To solve this model all the relevant physical and chemical processes, described in Section 2.4, were taken into account. The inlet and outlet concentration values were used to calculate overall fuel utilization. Fuel concentration profiles are plotted in Fig. 4a and b for 1:1 and 1:8 fuel-to-electrolyte flow rate ratios, respectively, at a total flow rate of 0.1 ml min^{-1}. The fuel concentration profiles were calculated for a LFFC operating at a cell potential of 0.3 V, the potential of maximum power density (Fig. 4a). At a flow rate ratio of 1:1, fuel crossover is evident, *i.e.*, [fuel] ~150 mM at the cathode near the end of the channel (Fig. 4a), but at a flow rate ratio of 1:8, the fuel stream is focused close the anode and fuel crossover is reduced significantly, *i.e.*, [fuel] ~7 mM at the cathode (Fig. 4b). As the oxygen concentration in air is only ~10 mM, the LFFC cathode operating at a 1:1 flow rate ratio (Fig. 4a) would perform very poorly because the fuel concentration at the cathode significantly exceeds the oxygen concentration over much of the length of the electrode. In contrast, when operating the LFFC at a 1:8 flow rate ratio, fuel crossover is barely an issue. Moreover, the fuel utilization is much higher when operating at a 1:8 flow rate ratio due to the absence of a lot of fuel in the middle of the channel, which in the 1:1 flow rate ratio operating condition flow through the cell without reacting. FEMLAB simulations for LFFCs operated at peak power density show that, fuel utilization efficiency improves from 25 to 54% when fuel-to-electrolyte flow rate ratios shift from 1:1 to 1:8, respectively.

FEMLAB simulations of formic acid concentration profiles were used to determine to fuel utilization values at total volumetric flow rates of 0.1 and 0.8 ml min^{-1} over a range of different fuel-to-electrolyte ratios. In Fig. 5a, these simulated values were compared to experimentally obtained results for a G2 LFFC, operated with formic acid. The corresponding experimental peak power densities for formic acid LFFCs are shown in Fig. 5b. The experimental and simulated fuel utilization results are in qualitative agreement as they exhibit similar trends. Deviations between the experimental and simulated results are observed at lower total flow rates and lower fuel-to-electrolyte flow rate ratios (corresponding to large difference between volumetric flow rates of the two streams). These deviations may be due, in part, to the adverse effects of fuel crossover, especially at lower total flow rates (longer residence times), which are not accounted for in the fuel utilization calculations. Also, experimental uncertainty, such as unsteady pumping, may impact performance especially at lower flow rate ratios. In general, after the fuel stream enters the LFFC, the concentration profile decreases due to the dual effects of: (i) fuel depletion at the anode, and (ii) diffusional broadening (*i.e.*, dilution) of the fuel stream into the cathodic stream. At a low total flow rate, fuel utilization was higher but peak power densities were lower. At a high total flow rate, fuel utilization was lower but peak power densities were higher. As previously noted, at a lower total flow rate, irrespective of fuel-to-electrolyte ratio, an increase in the fuel utilization is observed due to the longer residence time. At a higher total flow rate, an increase in peak power density is observed as a result of the thinner boundary layers that are rapidly replenished. In a similar vein, the fuel utilization decreases (Fig. 5a) and the peak power densities increases (Fig. 5b) when

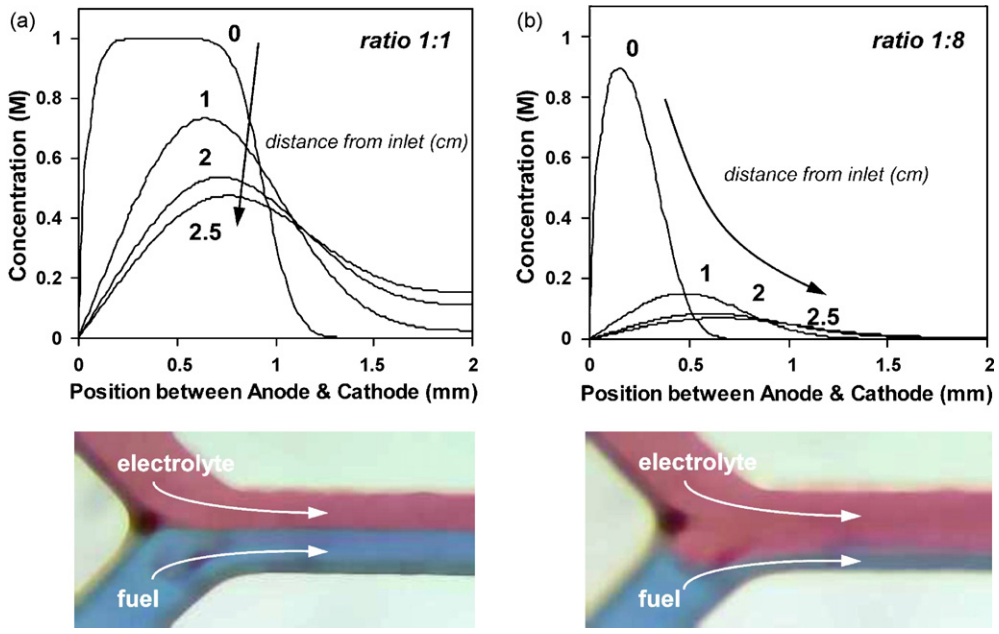

Fig. 4. Simulated concentration profiles of the fuel stream at different distances down the channel for a flow rate ratio of (a) 1:1 and (b) 1:8 at a total flow rate of 0.1 ml min^{-1}. The electrode-to-electrode distance was 0.2 cm. These curves were obtained at $Z = (1/2)H$, so at the center of the channel with a height H. For these simulations, the channel length, width and height are 2.5, 0.2, and 0.2 cm, respectively. Below each profile, optical micrographs of aqueous streams in laminar flow illustrate fuel-to-electrolyte flow rate ratios of 1:1 and 1:8, with the blue and red streams representing the fuel and electrolyte streams, respectively. Focusing of the fuel stream reduces fuel crossover and increases fuel utilization. (For interpretation of the references to color in this figure legend, the reader is referred to the web version of the article.)

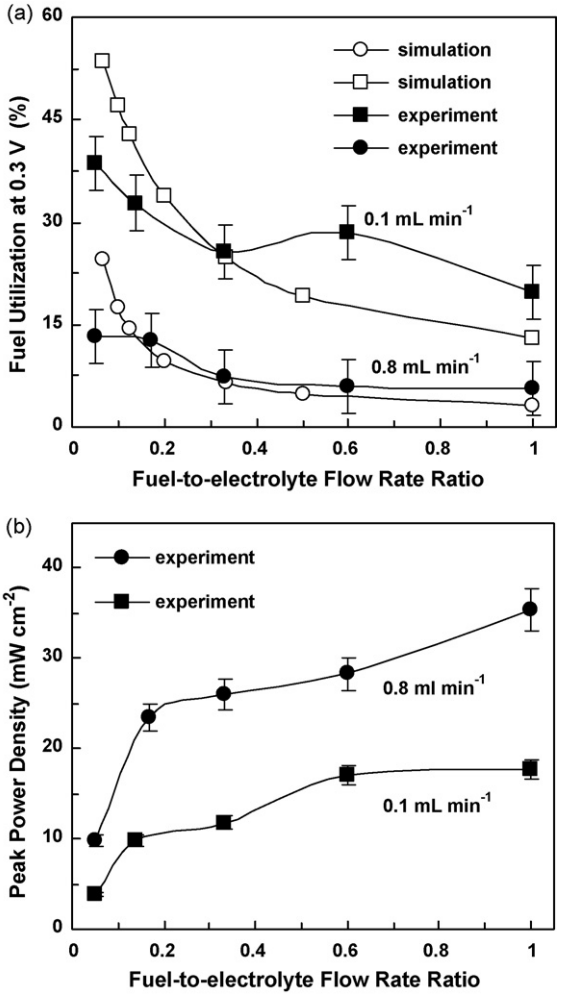

Fig. 5. (a) Simulated and experimental formic acid utilization and (b) peak power density as a function of fuel-to-electrolyte flow rate ratio, obtained in G2 LFFCs with a total flow rate of 0.1 and 0.8 ml min^{-1}. The anode stream was 1 M HCOOH + 0.5 M H_2SO_4 and the cathode stream was 0.5 M H_2SO_4. The electrode-to-electrode distance was 0.2 cm.

the fuel-to-electrolyte ratio is increased, irrespective of total flow rates.

At a 1:1 fuel-to-electrolyte ratio (maximum ratio), experimental peak power densities are 19 and 35 mW cm^{-2} were achieved for total flow rates of 0.1 and 0.8 ml min^{-1}, respectively. At high flow rate ratios, the larger fuel volume minimizes fuel depletion at the anode by maintaining high reactant fluxes to the catalytic surface. As mentioned above, increasing the total flow rate further reduces the depletion boundary layer thickness. Unfortunately, at these high ratios fuel utilization are lower, 24.5 and 7.5% for 0.1 and 0.8 ml min^{-1}, respectively, because the large fuel volumes that maintain the high reactant flow rates are not exhausted. At a 1:20 fuel-to-electrolyte ratio (minimum ratio), maximum experimental fuel utilization efficiencies of 38 and 14% were achieved for total flow rates of 0.1 and 0.8 ml min^{-1}, respectively. However at these low flow rate ratios (below 0.2), diffusional broadening effects dominate as the thin fuel stream is rapidly diluted into/by the electrolyte stream. An identical dilution effect is observed in Fig. 4 as the maxima of the simulated fuel concentration profiles at 1-cm from the channel entrance are 0.74 M and 0.17 M for flow rate ratios of 1:1 and 1:8, respectively. All these observation indicate that in order to improve fuel utilization while maintaining high peak performances, the LFFC channel length must be kept short, *e.g.* less than 0.5 cm, because most of the current will be collected over the first few millimeters of the electrode. In our previously reported work using unoptimized G2 LFFC designs, with total stream flow rates of 0.6 ml min^{-1} (at a 1:1 fuel-to-electrolyte ratio) and channel lengths of 2 cm, fuel crossover is minimal and does not significantly impact performance [23,24,26].

A number of fuel utilization studies have been performed on a variety of formic acid-based microfluidic fuel cells, which employ both innovative architectures and operating strategies [29,32,39–41]. These investigations report peak utilizations ranging from 23 to 86%, confirming that our hydrodynamic focusing technique is a simple and effective method for enhancing fuel utilization without specializing cell configuration. Structural modifications may also be used to increase fuel utilization, such as integrated microstructured ridges in the anode. Originally introduced by Stroock et al. [42], these ridges induce a helical flow pattern *within* the fuel stream, thereby replenishing the depletion boundary layer at the anode with fuel that has diffused away towards the channel center. In prior work, we demonstrated mass transfer to the anode can be enhanced at low fuel-to-electrolyte flow rate ratios by integrating ridges on the bottom of the microfluidic channel [43]. Using a model reaction, this passive replenishment mechanism resulted in a 10–40% increase in conversion. Additionally, fuel utilization can be further improved by altering overall cell architecture, such as high surface area flow-through and/or three-dimensional electrodes [44–46].Here, the qualitative agreement between experimental data and modeling indicates that simple models, such as this finite-element approach, can be used to guide the design of LFFCs. The ramifications of changes to the design (*i.e.*, dimensions, geometries) and/or operation conditions on fuel utilization and power density can be estimated before different LFFCs are being fabricated or different operation conditions are being tested experimentally. Outcomes of the modeling provide qualitative information on whether fuel utilization and/or power density will increase or decrease with changes in design or operation conditions. Furthermore, such modeling efforts allow a 1st order parameter sensitivity analysis, because identification of the parameters that have the biggest effect on LFFC performance will be straightforward.

3.4. LFFC performance as a function of electrode-to-electrode distance

The effect of electrode-to-electrode distance on the performance of G2 LFFCs was studied, as different electrode-to-electrode distances can significantly alter cell resistance and thus cell performance. Fig. 6a shows the polarization and power density curves for LFFCs, operated using 1 M HCOOH as the fuel, with 0.2 and 0.05 cm electrode-to-electrode distances. The volumetric flow rates used for electrode-to-electrode distances of 0.2 and 0.05 cm were 1.2 and 0.3 ml min^{-1}, respectively, to ensure the same average linear velocity remained ($v = 0.33$ cm s^{-1}). Under identical experimental conditions, peak power density increased from 26 to 35 mW cm^{-2} when the electrode-to-electrode distance was decreased from 0.2 to 0.05 cm. At the smaller distance, the shallower polarization curve indicates the improved LFFC performance is due to the reduced cell resistance.

3.5. LFFC performance as a function of flow rate

The effect of flow rate on the performance of G2 LFFCs was studied (Fig. 6). The performance in a LFFC with a 0.2-cm electrode-to-electrode distance remained constant when the average linear velocity was reduced by a factor of four from 0.33 to 0.075 cm s^{-1} (volumetric flow rate reduced from 1.2 to 0.3 ml min^{-1}, Fig. 6b), which indicates that at these flow rates, the performance of this cell is not mass transfer limited. However, LFFC performance

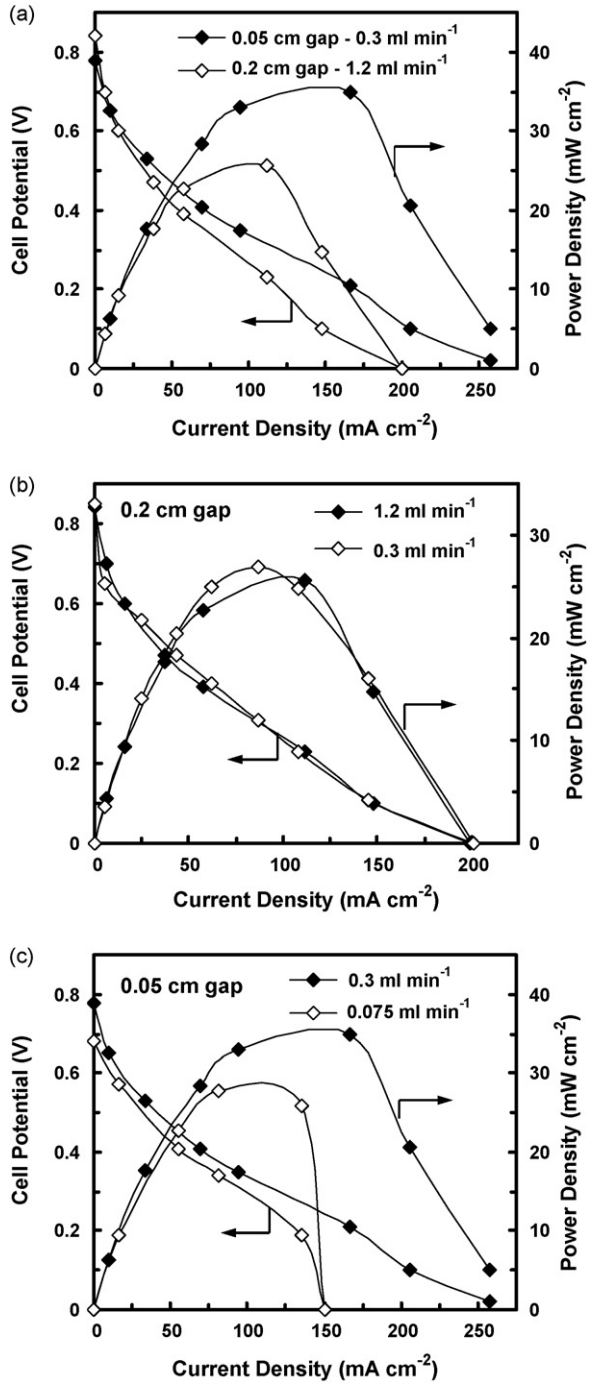

Fig. 6. Polarization and power density curves of G2 LFFCs operated with an anode stream of 1 M HCOOH + 0.5 M H_2SO_4 and a cathode stream of 0.5 M H_2SO_4: (a) two cells with electrode-to-electrode distances of 0.2 and 0.05 cm operated with total flow rates of 1.2 and 0.3 ml min^{-1}, respectively, so that the average linear velocity of 0.33 cm s^{-1} remains constant; (b) cell with a 0.2-cm electrode-to-electrode distance operated at two different total flow rates; and (c) cell with an 0.05-cm electrode-to-electrode distance operated at two different flow rates. In all studies, the fuel-to-electrolyte flow rate ratio was 1:1 and experiments were performed at room temperature.

with a 0.05-cm electrode-to-electrode distance was investigated decreasing the average linear velocity from 0.33 to 0.075 cm s^{-1} (volumetric flow rate decreased from 0.3 to 0.075 ml min^{-1}) led to a decrease in cell performance from 36 to 28 mW cm^{-2} (Fig. 6c). The onset of mass transfer limitations is evident from the sudden drop in potential at high current densities which can be explained by a significant increase in the boundary layer thickness, δ, which scales according to Eq. (6) [47].

$$\delta \propto \frac{Sc^{1/3} \cdot y}{\sqrt{Re_y}} \tag{6}$$

From this equation follows that a factor of four decrease in the linear velocity, z, leads to a doubling of the depletion boundary layer thickness, which impedes the reactant transport to the electrode.

3.6. LFFC performance as a function of oxidant supply

G2 LFFC performance is studied as a function of the flow rate and concentration of the gaseous oxygen delivered to the cathode. Fig. 7 compares the performance of LFFCs with the cathode exposed to (i) quiescent air and (ii) a 50 cm^3 s^{-1} stream of neat oxygen gas. As before, the volumetric flow rates used for electrode-to-electrode distances of 0.2 and 0.05 cm were 1.2 and 0.3 ml min^{-1}, respectively, to ensure constant linear velocities (v = 0.33 cm s^{-1}) such that the depletion boundary layer thickness is unchanged. Exposure of the cathode to the oxygen stream enhanced the performance by ~60% for both LFFCs: from 26 to 42 mW cm^{-2} for a 0.2-cm electrode-to-electrode distance (Fig. 7a) and from 35 to 55 mW cm^{-2} for a 0.05-cm electrode-to-electrode distance (Fig. 7b). The polarization curves in Fig. 7 exhibit significantly lower overpotentials for the forced oxygen cells compared to the air-

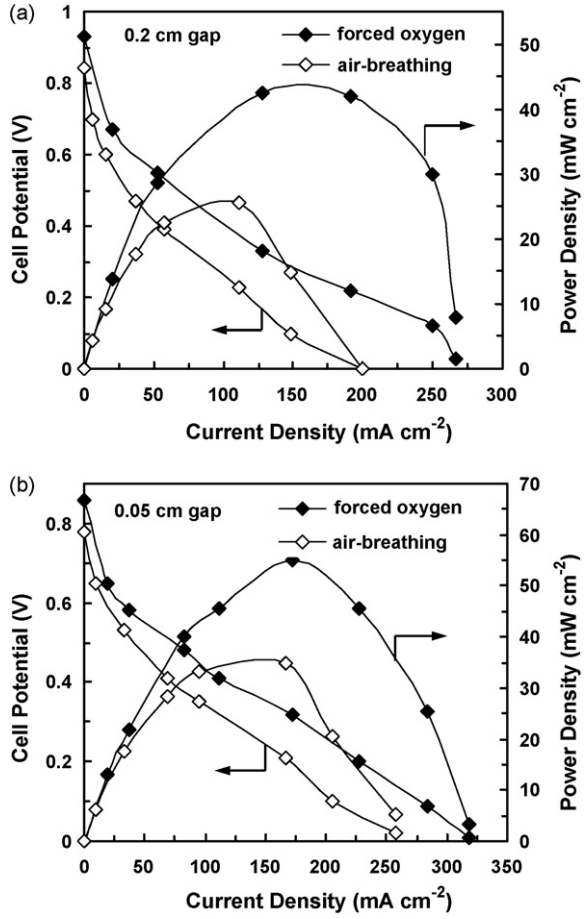

Fig. 7. Polarization and power density curves with an electrode-to-electrode distance of (a) 0.2 cm and (b) 0.05 cm operated with either forced oxygen at 50 cm^3 s^{-1} or quiescent air at the cathode. The anode and cathode streams were 1 M HCOOH + 0.5 M H_2SO_4 and 0.5 M H_2SO_4, respectively. To ensure identical linear velocities the total flow rates were 1.2 ml min^{-1} for (a) and 0.3 ml min^{-1} for (b). In all studies, the fuel-to-electrolyte ratio of 1:1 and experiments were performed at room temperature.

breathing cells as a result of the higher oxygen concentration on the cathode.

To further improve the power density one could imagine operating a forced oxygen LFFC at a fuel-to-electrolyte flow rate ratio of 1:8, like in Fig. 5b. Unfortunately, at these low flow rate ratios the performance of current LFFC configuration is limited by mass transfer at *the anode* as evidenced by the steady drop in performance as a function of decreasing fuel-to-electrolyte ratio (Fig. 5). Nevertheless, one could improve the LFFC performance by supplying the cathode with a forced oxygen stream (instead of quiescent air) to improve the individual electrode performance.

3.7. Power density versus fuel utilization trade-off

The membraneless architecture of laminar flow-based fuel cells (LFFCs) overcomes the fuel crossover and water management issues that plague membrane-based fuel cells (*i.e.*, PEMFC, DMFC) and enables independent control of stream characteristics (*i.e.*, flow-rate, composition, pH). Here we focused on maximizing cell performance, in terms of power density and fuel utilization per pass, by tailoring various structural and operational parameters, including absolute flow rate, fuel-to-electrolyte flow rate ratio, electrode-to-electrode distance, and oxygen concentration and mode of delivery.

The *power density* of a single LFFC can be optimized by reducing the electrode-to-electrode distance which lowers cell resistance. However, too small of an electrode-to-electrode gap will enhance fuel crossover, thus negatively affecting the *maximum* power density. Moreover, from a balance of plant (BOP) point of view, parasitic losses will increase as a result of increased pressure drop in narrower channels. Increasing the flow rates and/or the fuel concentration also increases the measured maximum power density since both improve mass transport to the anode through a thinner depletion boundary layer. Increasing the fuel concentration, however, increases the extent of fuel crossover, thus reversing the desired increase in power density. By optimizing each of these parameters, we achieved a peak power density of 55 mW cm^{-2} using 1 M HCOOH as the fuel in an LFFC with an electrode-to-electrode distance of 0.05 cm operated at a total stream flow rate of 0.3 ml min^{-1} (1:1 fuel-to-electrolyte ratio), and using a forced oxygen flow at the cathode. Yet, by increasing stream flow rates and flow rate ratios to maximize LFFC power density, fuel utilization is sacrificed. Reducing the channel length in the LFFC cell as well as improvements to the electrodes (*i.e.*, exact composition, preparation protocol), particularly of the anode, is expected to further enhance the performance of a single LFFC.

Fuel utilization is a second important performance metric of a fuel cell. By adjusting flow rate ratios between the fuel and the electrolyte streams in an LFFC, the fuel stream can be hydrodynamically focused into a thin layer on the anode. This approach eliminates the fraction of the fuel stream in the middle of the channel that typically passes through without reacting, and thus increases fuel utilization. In addition, the fuel utilization can be increased by reducing the absolute flow rate (longer residence times), yet this comes at the price of reduced power densities. The best fuel utilization per single pass approaching 40% we obtained for a LFFC operated at a fuel-to-electrolyte ratio of 1:20 and a total flow rate of 0.1 ml min^{-1}. Fuel utilization may be further improved by introducing ridges on the anode to increase mass transport to the catalytic surface.

4. Conclusions

Our results highlight the existence of a trade-off between maximizing power density and fuel utilization for LFFCs. High fuel utilization efficiencies are achieved at low flow rates and low fuel-to-electrolyte flow rate ratios, whereas cell performances are higher at high overall flow rates. The best combination of LFFC geometry and operation parameters can only be determined with an explicit intended application with specific power and operational lifetime requirements as well as weight and volume restrictions in mind [48]. First, to obtain a certain absolute power level, a certain number of individual LFFCs will need to be arranged in an array, *i.e.*, scaling out rather than scaling up to maintain the laminar flow regime. Second, one can run a larger number of LFFCs at lower power density but optimized fuel utilization in a single pass to avoid having to integrate the capability to recirculate the fluids within the BOP. Alternatively, one can run fewer cells at higher power density but low fuel utilization per pass (say 50%) in a fuel and electrolyte recirculation scenario. The latter case would make more sense for a larger system that is desired to run for an extended period of time. A system level analysis and optimization effort is needed taking into account the parameters that determine the performance of a single LFFC as well as all aforementioned parameters that will determine the overall performance and specifications of the system. The development and continued improvement of individual LFFC models, presently for fuel utilization per pass but also for power density in the near future, will facilitate these efforts by enabling rapid characterization of cell performance as a function of all possible permutations of relevant parameters.

Acknowledgements

This work was supported through an STTR Phase II grant from ARO to INI Power Systems of Morrisville, NC and the University of Illinois at Urbana-Champaign (contract no. W911NF-04-C-113). Financial support by the University of Illinois and by NSF for a CAREER award to PJAK (CTS 05-47617) as well as by Graduate Engineering for Minorities (GEM) Fellowship for FRB are also gratefully acknowledged. The authors thank Dr. Lajos Gancs, Dr. Wei-Ping Zhou, Daniela Egas, Matthew Naughton and Joshua Tice for stimulating discussions.

References

[1] A. Kundu, J.H. Jang, J.H. Gil, C.R. Jung, H.R. Lee, S.H. Kim, B. Ku, Y.S. Oh, J. Power Sources 1 (2007) 67–78.
[2] S.C. Kelley, G.A. Deluga, W.H. Smyrl, Electrochem. Solid-State Lett. 9 (2000) 407–409.
[3] C. Rice, S. Ha, R.I. Masel, P. Waszczuk, A. Wieckowski, T. Barnard, J. Power Sources 1 (2002) 83–89.
[4] K. Shah, W.C. Shin, R.S. Besser, Sens. Actuators, B 2–3 (2004) 157–167.
[5] Z.P. Shao, S.M. Haile, J. Ahn, P.D. Ronney, Z.L. Zhan, S.A. Barnett, Nature 7043 (2005) 795–798.
[6] N. Mano, F. Mao, A. Heller, J. Am. Chem. Soc. 21 (2003) 6588–6594.
[7] R.L. Arechederra, S.D. Minteer, Fuel Cells 1 (2009) 63–69.
[8] J. Yeom, G.Z. Mozsgai, B.R. Flachsbart, E.R. Choban, A. Asthana, M.A. Shannon, P.J.A. Kenis, Sens. Actuators, B 2 (2005) 882–991.
[9] C. Apblett, D. Ingersoll, P. Atanassov, D. Maricle, S. Sarangapani, J. Power Sources 1 (2006) 255–261.
[10] S. Tominaka, S. Ohta, H. Obata, T. Momma, T. Osaka, J. Am. Chem. Soc. 32 (2008) 10456–10457.
[11] E. Kjeang, N. Djilali, D. Sinton, J. Power Sources 2 (2009) 353–369.
[12] L. Carrette, K.A. Friedrich, U. Stimming, Chemphyschem 4 (2000) 162–193.
[13] M.L. Perry, T.F. Fuller, J. Electrochem. Soc 7 (2002) S59–S67.
[14] U.B. Demirci, J. Power Sources 2 (2007) 239–246.
[15] G.Q. Lu, C.Y. Wang, T.J. Yen, X. Zhang, Electrochim. Acta 5 (2004) 821–828.
[16] X.M. Ren, S. Gottesfeld, Air breathing direct methanol fuel cell, U.S. Patent 6,458,479, 1 October (2002).
[17] Y.M. Zhu, S.Y. Ha, R.I. Masel, J. Power Sources 1–2 (2004) 8–14.
[18] Y.W. Rhee, S.Y. Ha, R.I. Masel, J. Power Sources 1–2 (2003) 35–38.
[19] P.J.A. Kenis, R.F. Ismagilov, G.M. Whitesides, Science 5424 (1999) 83–85.
[20] E.R. Choban, P. Waszczuk, P.J.A. Kenis, Electrochem. Solid-State Lett. 7 (2005) A348–A352.
[21] E.R. Choban, L.J. Markoski, A. Wieckowski, P.J.A. Kenis, J. Power Sources 1 (2004) 54–60.
[22] E.R. Choban, J.S. Spendelow, L. Gancs, A. Wieckowski, P.J.A. Kenis, Electrochim. Acta 27 (2005) 5390–5398.
[23] R.S. Jayashree, L. Gancs, E.R. Choban, A. Primak, D. Natarajan, L.J. Markoski, P.J.A. Kenis, J. Am. Chem. Soc. 48 (2005) 16758–16759.

[24] R.S. Jayashree, D. Egas, J.S. Spendelow, D. Natarajan, L.J. Markoski, P.J.A. Kenis, Electrochem. Solid-State Lett. 5 (2006) A252–A256.
[25] D.T. Whipple, R.S. Jayashree, D. Egas, N. Alonso-Vante, P.J.A. Kenis, Electrochim. Acta 18 (2009) 4384–4388.
[26] F.R. Brushett, R.S. Jayashree, W.P. Zhou, P.J.A. Kenis, Electrochim. Acta 27 (2009) 7099–7105.
[27] L.J. Markoski, P.J.A. Kenis, E.R. Choban, Fuel cells comprising laminar flow induced dynamic conducting interfaces, electronic devices comprising such cells and methods employing same, US Patent Office 7,252,898, 7 August (2007).
[28] S.M. Mitrovski, L.C.C. Elliott, R.G. Nuzzo, Langmuir 17 (2004) 6974–6976.
[29] A. Bazylak, D. Sinton, N. Djilali, J. Power Sources 1–2 (2005) 57–66.
[30] J.L. Cohen, D.J. Volpe, D.A. Westly, A. Pechenik, H.D. Abruna, Langmuir 8 (2005) 3544–3550.
[31] M.H. Sun, G.V. Casquillas, S.S. Guo, J. Shi, H. Ji, Q. Ouyang, Y. Chen, Microelectron. Eng. (2007).
[32] D.H. Ahmed, H.B. Park, H.J. Sung, J. Power Sources 1 (2008) 143–152.
[33] R.F. Ismagilov, A.D. Stroock, P.J.A. Kenis, G. Whitesides, H.A. Stone, Appl. Phys. Lett. 17 (2000) 2376–2378.
[34] J.B. Knight, A. Vishwanath, J.P. Brody, R.H. Austin, Phys. Rev. Lett. (1998) 3863–3866.
[35] S.K. Yoon, E.R. Choban, C. Kane, T. Tzedakis, P.J.A. Kenis, J. Am. Chem. Soc. 30 (2005) 10466–10467.
[36] N.M. Markovic, P.N. Ross Jr., in: A. Wieckowski (Ed.), Interfacial Electrochemistry: Theory, Experiment, and Applications, Marcel Dekker, New York, 1999, pp. 821–841.
[37] J. Jiang, A. Kucernak, J. Electroanal. Chem. 1–2 (2002) 64–70.
[38] L.J. Markoski, P. Waszczuk, P.J.A. Kenis, E.R. Choban, Emulsions for fuel cells, US Patent 7,205,064, 27 June (2003).
[39] J. Phirani, S. Basu, J. Power Sources 1 (2008) 261–265.
[40] H.B. Park, D.H. Ahmed, K.H. Lee, H.J. Sung, Electrochim. Acta 18 (2009) 4416–4425.
[41] K.S. Salloum, J.R. Hayes, C.A. Friesen, J.D. Posner, J. Power Sources 1 (2008) 243–252.
[42] A.D. Stroock, S.K.W. Dertinger, A. Ajdari, I. Mezic, H.A. Stone, G.M. Whitesides, Science 5555 (2002) 647–651.
[43] S.K. Yoon, G.W. Fichtl, P.J.A. Kenis, Lab Chip 12 (2006) 1516–1524.
[44] E. Kjeang, J. McKechnie, D. Sinton, N. Djilali, J. Power Sources 2 (2007) 379–390.
[45] E. Kjeang, R. Michel, D.A. Harrington, N. Djilali, D. Sinton, JACS 12 (2008) 4000–4006.
[46] E. Kjeang, B.T. Proctor, A.G. Brolo, D.A. Harrington, N. Djilali, D. Sinton, Electrochim. Acta 15 (2007) 4942–4946.
[47] G. Prentice, Electrochemical Engineering Principles, Prentice Hall, Englewood Cliffs, NJ, 1991.
[48] A.S. Hollinger, R.J. Maloney, R.S. Jayashree, D. Natarajan, L.J. Markoski, P.J.A Kenis, J. Power Sources (2010), in press.